Spin-polarized ground states and ferromagnetic order induced by low-coordinated surface atoms and defects in nanoscale magnesium oxide

Uchino, Takashi

Yoko, Toshinobu

Spin-polarized ground states and ferromagnetic order induced by low-coordinated surface atoms and defects in nanoscale magnesium oxide

Takashi Uchino*
Department of Chemistry, Graduate School of Science, Kobe University, Nada, Kobe 657-8501, Japan

Toshinobu Yoko
Institute for Chemical Research, Kyoto University, Uji, Kyoto 611-0011, Japan

(Received 13 July 2012; revised manuscript received 23 February 2013; published 18 April 2013)

We investigate the effect of surface defects and the related low-coordinated surface atoms on the defect-induced magnetism in MgO nanocrystallites using hybrid density functional theory calculations. It has been demonstrated that when Mg vacancies are introduced at the surface or near surface of cubelike MgO clusters, a magnetic state ($S \geqslant 1$) becomes lower in total energy than the nonmagnetic singlet state ($S = 0$) by several electron volts, resulting in the robust spin-polarized ground state. The total spin S of the clusters in their ground state is equal to the number of the surface Mg vacancies introduced. The resulting spin density is not only located at the surrounding O atoms neighbor to the Mg vacancy site but is also extended to the low-coordinated surface O atoms along the ⟨110⟩ direction, forming ferromagneticlike domains. This directional spin delocalization allows a remote (∼1 nm or longer) vacancy-vacancy interaction, eventually leading to a long-range ferromagnetic interaction.

DOI: 10.1103/PhysRevB.87.144414 PACS number(s): 75.70.Cn, 75.47.Lx, 75.70.Rf, 75.75.Lf

I. INTRODUCTION

Recent progress in materials synthesis has led to a variety of nanostructures whose optical, electrical, and magnetic properties are very different from those of bulk structures. This also reveals anomalous aspects of well-understood phenomena of condensed matter physics. One of the interesting examples of the anomalies found in nanoscale oxides is the so-called d^0 ferromagnetism,[1] which is referred to as small but nonnegligible ferromagnetic moments observed in closed shell oxide systems, e.g., HfO_2 (Ref. 2), TiO_2 (Refs. 3 and 4), CeO_2 (Ref. 5), ZnO (Ref. 5), Al_2O_3 (Ref. 5), and MgO (Refs. 5–8), containing virtually no atoms with partially filled d or f shells. This intriguing ferromagnetism occurs even at temperatures well above room temperature and seems to exist outside the conventional m-J paradigm,[1,9,10] where m and J represent the magnetic moment and the exchange coupling of electron spins, respectively. Thus far, the d^0 ferromagnetism has been observed almost universally in nanoscale oxides and is believed to result from magnetic moments related to a certain defective state.[7–13] However, a simple defect-based model cannot account for the observed ferromagnetic behavior because of a rather localized nature of the relevant defect orbitals, which will be insufficient to induce long-range ferromagnetic order, as has been shown by recent density functional theory (DFT) calculations, including electronic correlation effects beyond standard (semilocal) DFT functionals.[14–16]

As for the mechanism of d^0 ferromagnetism, we[17] have recently shown from the DFT calculations on a series of MgO clusters that some crystallographically perfect nanocrystallites paradoxically result in nonstoichiometric compositions owing the finite number of constituting atoms, resulting in a spin-triplet ground state. On the basis of the calculations, we proposed an idea that ferromagnetism in nanoscale oxides can arise from the combined effect of crystal symmetry and inherent nonstoichiometry. We believe that this idea is appealing in some ways, but this cannot give an answer as to how the localized defect states are linked and coupled, showing a collective ferromagnetic ordering.

When we say "defects" in oxides, we usually mean "atomic defects," e.g., vacant atom sites, interstitial atoms, or substitution of a foreign atom for a normal one, in the bulk. Thus, previous theoretical calculations on defect-related ferromagnetism have been performed mainly on the atomic defects in the bulk using supercell methods.[7,14,15,18] However, all the atoms at the surface can also be regarded as structural defects or imperfections because of the reduced number of coordination bonds. As for nanoscale oxides, the possible effect of these surface atoms may not be completely neglected. Furthermore, it has been demonstrated that the low-coordinated surface sites, such as terraces, edges, and corners, are more stable locations for atomic defects than the bulk sites because the formation energy of atomic defects will decrease with the decreasing number of surrounding atoms.[19,20] This allows one to expect that these low-coordinated surface states could potentially contribute to the generation of defect-related ferromagnetism in nanoscale oxide, as suggested by recent observations.[6,8,21] However, the possible surface effects on the defect-related magnetism have not been well investigated theoretically.[18]

We hence carry out a series of quantum chemical DFT calculations on isolated MgO clusters with surface atomic defects, including O and Mg vacancies. Such isolated cluster models are not appropriate to investigate the electronic structure of the bulk system and the extended surface of crystals. When materials are reduced to the nanoscale, however, their structure and properties can deviate from the bulk or extended surface case. Accordingly, real space cluster models, rather than reciprocal space description, will become more effective in addressing, especially, surface-related phenomena in nanocrystals.

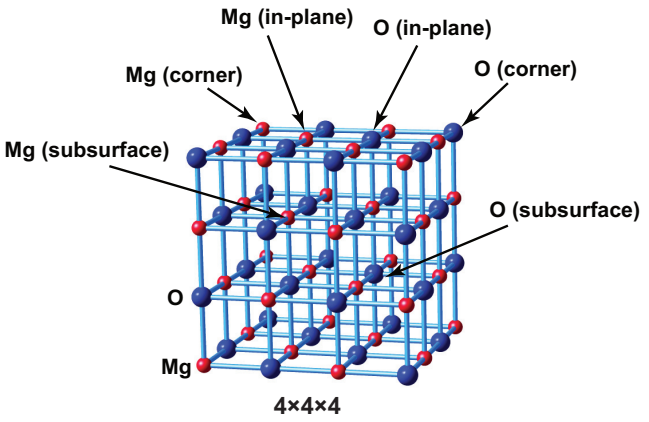

FIG. 1. (Color online) (a) Schematic view of a $(4 \times 4 \times 4)$-atom block of the MgO cluster. An Mg (or O) atom, indicated by an arrow, is removed to create an Mg- (or O-) deficient cluster.

II. MODELS AND CALCULATION PROCEDURES

As for MgO clusters with more than ∼50 atoms, it has been demonstrated that the cubic rock-salt structure thermodynamically dominates the energy landscape.[22] We hence employed several top-down clusters based on cuts from the cubic rock-salt structure as representative models of nanometer-sized MgO crystals. We first consider a $(4 \times 4 \times 4)$-atom block of stoichiometric $Mg_{32}O_{32}$ cluster consisting of 64 atoms, as shown in Fig. 1. To evaluate the possible effect of location of the Mg (or O) vacancy site on the stable spin state we intentionally removed one Mg (or O) atom from a three-coordinated (corner), a five-coordinated (in-plane), or a six-coordinated (subsurface) site of the $4 \times 4 \times 4$ cluster. We then performed full geometry optimization for the respective Mg-deficient ($Mg_{31}O_{32}$) and O-deficient ($Mg_{32}O_{31}$) clusters, starting from ideal cubic configurations at the singlet ($S = 0$) and triplet ($S = 1$) spin states without imposing any structural constraints. As for the spin-singlet calculations, we used both the spin-restricted DFT (RDFT) and broken-symmetry spin-unrestricted DFT (UDFT) formalisms. All the DFT calculations in this work were carried out using the gradient-corrected Becke's three parameters hybrid exchange functional[23] in combination with the correlation functional of Lee, Yang, and Parr[24] (B3LYP) with the GAUSSIAN-09 code.[25] It has previously been shown that such a hybrid DFT functional is useful to correct the self-interaction problem,[26] which often leads to misleading conclusions with regards to hole localization and the resulting magnetic characteristics of the system.[16,27] Mulliken's population analysis was conducted to calculate the spin densities of the clusters at B3LYP/6-31G(d) level. The stability of the resulting optimized clusters was evaluated in terms of the total energy along with the atomization energy (AE), which is defined as the energy necessary to dissociate the Mg_mO_n cluster into neutral atoms (mMg + nO), namely, AE $= mE(\mathrm{Mg}) + nE(\mathrm{O}) - E(\mathrm{Mg}_m\mathrm{O}_n)$, where $E(\mathrm{X})$ represents the total energy of the system X. The AE is useful to evaluate the stability of the clusters with the same dimension but different compositions and spin states.

Furthermore, we employed a series of Mg-deficient clusters consisting of $(4 \times 4 \times 4)$-, $(6 \times 4 \times 3)$-, $(7 \times 4 \times 3)$-, and $(8 \times 4 \times 3)$-atom blocks to investigate whether the defect-induced spin polarization can couple ferromagnetically with each other. For that purpose we removed two corner Mg atoms located in the same (100) plane of the respective

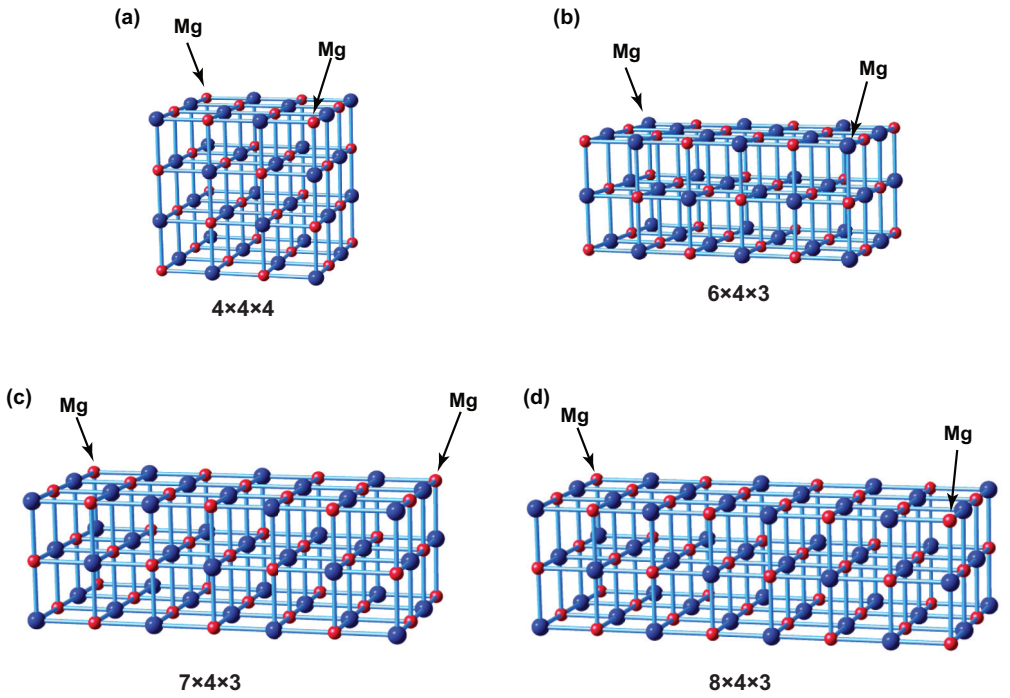

FIG. 2. (Color online) Schematic views of (a) $(4 \times 4 \times 4)$-, (b) $(6 \times 4 \times 3)$-, (c) $(7 \times 4 \times 3)$-, and (d) $(8 \times 4 \times 3)$-atom blocks of the MgO clusters. Two corner Mg atoms indicated by arrows are removed from each cluster to create the corresponding Mg deficient cluster with two Mg vacancies.

TABLE I. Electronic properties of the (4 × 4 × 4)-based MgO cluster with one Mg or one O vacancy at different sites. Geometry optimization was performed at the B3LYP/6-31G(d) level in the respective spin states.

Cluster	Spin State	ΔE[a](eV)	AE[b](eV)	$\langle S^2\rangle$[c]	$\Delta E_{\mathrm{H-L}}$[d](eV)
		$Mg_{32}O_{31}$			
corner O vacancy	singlet (R)[e]	–	270.588	0	1.68
	singlet (U)[f]	0	270.588	0	1.68(α)/1.68(β)
	triplet	+1.005	269.583	2.002(2.000)	0.40(α)/3.38(β)
in-plane O vacancy	singlet (R)	–	269.258	0	1.68
	singlet(U)	0	269.258	0	1.68(α)/1.68(β)
	triplet	+0.691	268.567	2.003(2.000)	0.44(α)/3.58(β)
subsurface O vacancy	singlet (R)	–	268.684	0	1.59
	singlet (U)	0	268.684	0	1.59(α)/1.59(β)
	triplet[g]	–	–	–	–
		$Mg_{31}O_{32}$			
corner Mg vacancy	singlet (R)	–	269.409	0	0.47
	singlet (U)	−1.261	270.670	1.014(0.112)	0.98(α)/1.35(β)
	triplet	−1.303	270.712	2.020(2.000)	3.97(α)/1.00 (β)
in-plane Mg vacancy	singlet (R)	–	268.654	0	0.40
	singlet (U)	−1.134	269.788	1.008(0.118)	1.41(α)/1.40(β)
	triplet	−1.133	269.787	2.015(2.000)	3.63 (α)/1.25(β)
subsurface Mg vacancy	singlet (R)	–	268.495	0	0.49
	singlet (U)	−0.984	269.479	1.017(0.136)	1.54(α)/0.54(β)
	triplet	−0.985	269.480	2.017(2.000)	3.89(α)/0.44(β)

[a]ΔE represents the total energy difference from the spin-restricted singlet state. Plus and minus signs indicate that the total energy is higher and lower, respectively, than that of the spin-restricted singlet state.
[b]AE (Atomization Energy) $= mE(\mathrm{Mg}) + nE(\mathrm{O}) - E(\mathrm{Mg}_m\mathrm{O}_n)$, where $E(\mathrm{X})$ represents the total energy of the system X.
[c]The values in parentheses are those after annihilation of the first spin contaminant.
[d]$\Delta E_{\mathrm{H-L}}$ is the energy difference between the HOMO and the LUMO levels. α and β indicate the major and minor spin states, respectively.
[e]Spin-restricted singlet state.
[f]Broken-symmetry spin-unrestricted singlet state.
[g]The Self-consisent field (SCF) did not converge for this cluster in the triplet state.

clusters, resulting in the $Mg_{30}O_{32}$, $Mg_{34}O_{36}$, $Mg_{40}O_{42}$, and $Mg_{46}O_{48}$ clusters (see Fig. 2). Full geometry optimizations were performed as well for this series of Mg-deficient clusters at the B3LYP/6-31G(d) level by assuming that $S = 0$, 1, and 2.

III. RESULTS

A. The (4 × 4 × 4) cluster with one Mg or O vacancy

First we show the results of the (4 × 4 × 4)-atom block of the clusters containing one Mg or one O vacancy. Although a slight outward displacement of the atoms surrounding each vacancy site was seen, the starting cubic configuration was basically retained after full geometry optimization for all the clusters employed irrespective of the assumed spin state. It should be noted, however, that the stability of the spin state varies depending on the type and location of the defect included in the cluster (see Table I).

As for the O-deficient ($Mg_{32}O_{31}$) clusters in the singlet ($S = 0$) state, the spin-restricted and spin-unrestricted singlet calculations gave identical ground state energies and molecular orbital structures. As shown in Fig. 3(a), the cluster with a corner O vacancy in the (spin-restricted) singlet state results in the lowest energy state among the present series of $Mg_{32}O_{31}$ clusters. This shows that the introduction of a surface O vacancy will not induce a spin-polarized ground state, which is in agreement with the results deduced from previous supercell calculations.[18,28]

As for the Mg-deficient ($Mg_{31}O_{32}$) cluster, however, the total energy of the spin-unrestricted singlet state is lower than that of the spin-restricted singlet state by ∼1 eV (see Table I). The apparent high energy of the spin-restricted state is attributed to an overestimate of on-site Coulomb repulsion, which is corrected in the unrestricted spin calculations. Note also that the total energy of the spin-unrestricted singlet state is almost comparable to that of the spin triplet state [see also Fig. 3(b)]. However, the spin-unrestricted singlet calculations yield the spin-squared expectation values $\langle S^2\rangle$ of ∼0.1 even after annihilation of the first spin contaminant (see also Table I), suggesting that the present UDFT singlet calculations are affected by the spin contamination problem,[29] as will be discussed in Sec. IV A.

Figure 4 illustrates the spin-magnetization density, which is defined as the local density difference between the spin-up and spin-down states, of the $Mg_{31}O_{32}$ cluster with a corner Mg vacancy in the spin-unrestricted singlet state and the spin triplet state. In both the spin states shown in Fig. 4, the spin is not only distributed over the three oxygen atoms next to the Mg vacancy site but also spreads further out of the nearest-neighbor oxygen atoms along the ⟨110⟩ direction on the {100} surface, showing a highly delocalized nature of the spin distribution. Of particular interest is the spin distribution of the spin-unrestricted singlet state. The spin distribution is not that of the usual antiferromagnetic state where the two adjacent electrons are in a spin-paired or antiparallel configuration;

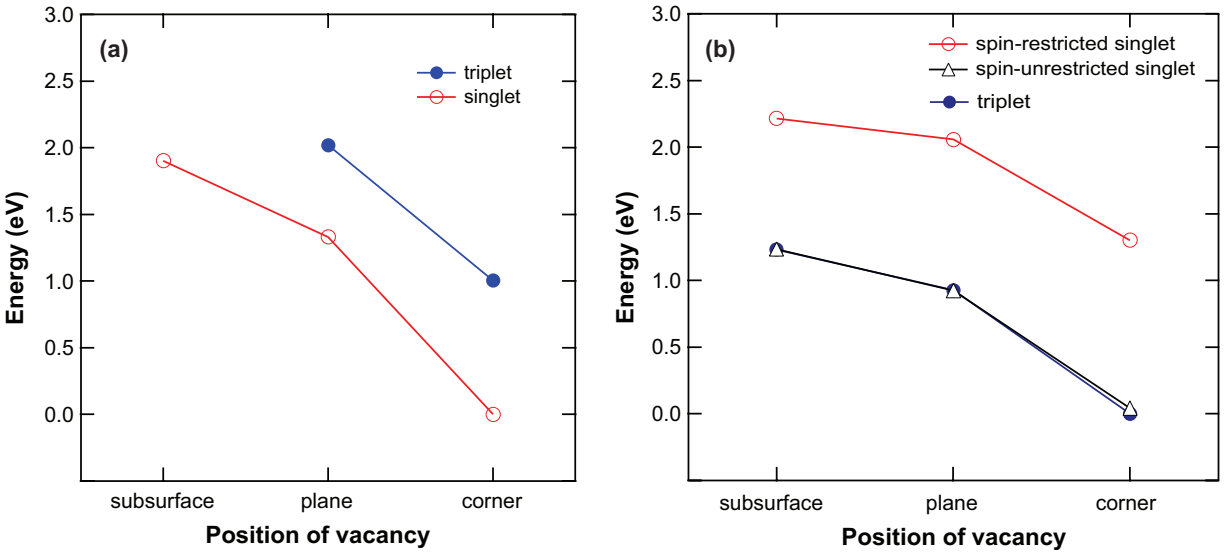

FIG. 3. (Color online) Comparison of the relative total energies of the (4 × 4 × 4)-based clusters with (a) one O vacancy and (b) one Mg vacancy located at different sites. For the O-deficient clusters, the energy is referenced to that of the cluster with a corner O vacancy in the spin-restricted singlet state. For the Mg-deficient clusters, the energy is referenced to that of the cluster with a corner Mg vacancy in the triplet state.

rather, this is reminiscent of the magnetic domains with opposing magnetizations [see Fig. 4(a)]. Strictly speaking, the resulting spin distribution is not ferromagnetic because the net magnetization is zero. However, the domainlike structure realized in the spin-unrestricted singlet state implies that the introduction of a surface Mg vacancy yields a kind of magnetic order.

It should be worth mentioning that this surface spin delocalization can also be seen when an Mg vacancy is introduced at the in-plane site [see Fig. 5(b)] or at the subsurface [see Fig. 5(c)]. This directional spin localization on the surface O atoms contrasts sharply with the results of supercell calculations on an Mg vacancy in the bulk, where strong localization of the spin density on one of the six O atoms around the Mg vacancy occurs as a result of a polaronic distortions and the resulting symmetry breaking around the vacancy site.[15] In the present clusters, the symmetry around the vacancy site is inherently broken, which might allow us to expect the strong localization of spin solely on the specific oxygen atoms surrounding the Mg vacancy. The apparently unexpected delocalization of the spin density presented here suggests that the energy levels of some of the surface low-coordinated O atoms are comparable to or even higher than those of the O atoms surrounding the vacancy. Consequently, these low-coordinated surface atoms will behave as "good hole acceptors," as will also be discussed in Sec. IV B.

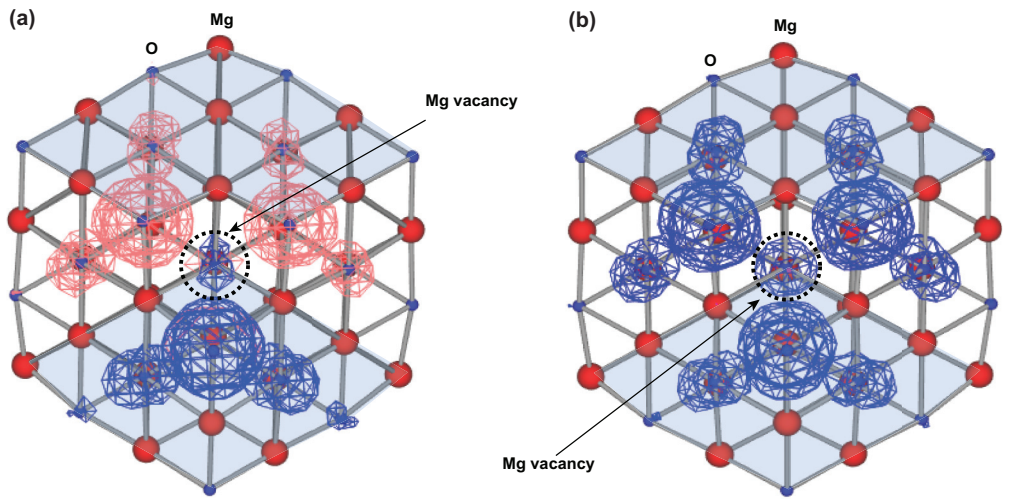

FIG. 4. (Color online) Spin-density isosurface (0.001 e/Bohr^3) projected from the [111] direction of the (4 × 4 × 4)-based cluster with one corner Mg vacancy calculated for (a) the spin-unrestricted singlet state and (b) the spin triplet state. Large and small circles represent Mg and O atoms, respectively. The corner Mg vacancy is located at the forward most position along the [111] direction. The blue (dark) and red (light) isosurfaces represent spin up and down values, respectively.

TABLE II. Electronic properties of various MgO-type clusters with two corner Mg vacancies optimized at the B3LYP/6-31G(d) level in the respective spin states.

Cluster	Spin State	ΔE[a](eV)	AE[b](eV)	$\langle S^2\rangle$[c]	$\Delta E_{\mathrm{H-L}}$[d](eV)
$Mg_{30}O_{32}$	singlet (R)[e]	–	261.701	0	0.46
$(4 \times 4 \times 4)$	singlet (U)[f]	−1.219	262.919	1.013 (0.101)	1.12 (α)/1.38(β)
	triplet	−1.354	263.055	3.026 (2.055)	1.65 (α)/1.20(β)
	quintet	−1.362	263.063	6.028 (6.000)	4.20 (α)/1.18(β)
$Mg_{34}O_{36}$	singlet (R)	–	295.904	0	0.59
$(6 \times 4 \times 3)$	singlet (U)	−2.639	298.542	2.023 (4.245)	1.75 (α)/1.24(β)
	triplet	−2.643	298.547	3.020 (2.045)	1.34 (α)/1.31(β)
	quintet	−2.646	298.550	6.023 (6.000)	4.36 (α)/1.22(β)
$Mg_{40}O_{42}$	singlet (R)	–	350.281	0	0.64
$(7 \times 4 \times 3)$	singlet (U)	−2.668	352.949	2.024 (4.261)	1.85 (α)/1.40(β)
	triplet	−2.669	352.950	3.024 (2.045)	1.41 (α)/1.40(β)
	quintet	−2.673	352.954	6.024 (6.000)	4.36 (α)/1.39(β)
$Mg_{46}O_{48}$	singlet (R)	–	404.873	0	0.64
$(8 \times 4 \times 3)$	singlet (U)	−2.685	407.558	2.024 (4.259)	1.45 (α)/1.45(β)
	triplet	−2.687	407.560	3.024 (2.049)	1.80 (α)/1.43(β)
	quintet	−2.690	407.563	6.024 (6.000)	4.35 (α)/1.43(β)

[a] ΔE represents the total energy difference from the spin-restricted singlet state. Minus signs indicate that the total energy is lower than that of the spin-restricted singlet state.
[b] AE (Atomization Energy) $= mE(\mathrm{Mg}) + nE(\mathrm{O}) - E(\mathrm{Mg}_m\mathrm{O}_n)$, where $E(\mathrm{X})$ represents the total energy of the system X.
[c] The values in parentheses are those after annihilation of the first spin contaminant.
[d] $E_{\mathrm{H-L}}$ is the energy difference between the HOMO and the LUMO levels. α and β indicate the major and minor spin states, respectively.
[e] Spin-restricted singlet state.
[f] Broken-symmetry spin-unrestricted singlet state.

B. Clusters with two Mg vacancies

We next investigate the structure and spin sates of $(4 \times 4 \times 4)$-, $(6 \times 4 \times 3)$-, $(7 \times 4 \times 3)$-, and $(8 \times 4 \times 3)$ clusters with two Mg vacancies at two end corners of the respective clusters. Similar to the case of the $(4 \times 4 \times 4)$ cluster with one Mg vacancy, we found that the original cubiclike configuration is retained as well after geometry optimization. The intervacancy distances for the optimized $(4 \times 4 \times 4)$-, $(6 \times 4 \times 3)$-, $(7 \times 4 \times 3)$-, and $(8 \times 4 \times 3)$ clusters are estimated to be ∼8.5, ∼12.0, ∼12.5, and ∼15.5 Å, respectively, and the relative total energies of the spin-unrestricted states with respect to the spin-restricted singlet ($S = 0$) state are summarized in Table II.

One sees from Table II that all these Mg-deficient clusters are characterized by the same the energetic ordering of different spin states, namely, $E_Q < E_T < E_{US} < E_{RS}$, where E_Q, E_T, E_{SU}, and E_{SR} represent the total energy of the spin-quintet, triplet, spin-unrestricted singlet, and spin-restricted singlet states, respectively. The spin-quintet and spin-restricted singlet states are separated by an energy of more than 1 eV, implying the existence of a stable spin-polarized state. Table II also shows that the spin-unrestricted singlet and spin triplet states are only slightly higher in energy (several milli-electron volts) than the spin-quintet state. However, the spin-unrestricted singlet and triplet states are found to be contaminated by higher spin states; that is, the $\langle S^2\rangle$ values are different from 0 (pure singlet) or 2 (pure triplet). On the other hand, the $\langle S^2\rangle$ value for the spin quintet ($S = 2$) states is 6.000 (after annihilation of the first spin contaminant), which corresponds to the ideal value $S(S + 1) = 6$.

Figure 6 compares the spin-magnetization density of the clusters with two corner Mg vacancies in the spin-quintet state. The directional spin delocalization is also seen in this series of clusters, in basic agreement with the results obtained for the clusters with one Mg vacancy, mentioned previously. It should also be worth mentioning that in the $(4 \times 4 \times 4)$ cluster, as shown in Fig. 6(a), the magnetic interaction between the two Mg vacancies can be explicitly recognized, showing a highly delocalized and extended nature of the spin polarization of the surface O atoms aligned along the ⟨110⟩ direction. The degree of intervacancy interaction appears to decrease with increasing the distance between a pair of Mg vacancies, but the directional spin delocalization over the surface O atoms still survives even in the $(8 \times 4 \times 3)$-based $Mg_{46}O_{48}$ cluster [see Fig. 6(d)]. This demonstrates that the surface O atoms indirectly but inherently contribute to the ferromagnetic interaction between rather remote-surface Mg vacancies, leading to the ferromagnetic percolation in MgO nanocrystals. Note also that the delocalized and domainlike spin distribution can also be seen in the spin-unrestricted singlet states for the clusters with two Mg vacancies (see, for example, Fig. 7). Thus, we consider that the ferromagnetic interaction between two surface Mg vacancies is not an artifact derived from the calculations for magnetic states with $S \geqslant 1$.

IV. DISCUSSION

A. Effect of the spin contamination and the number of Mg vacancies on the magnetic states of the Mg-deficient clusters

For all the Mg-deficient clusters investigated in this work, it has been demonstrated that spin-unrestricted states are lower

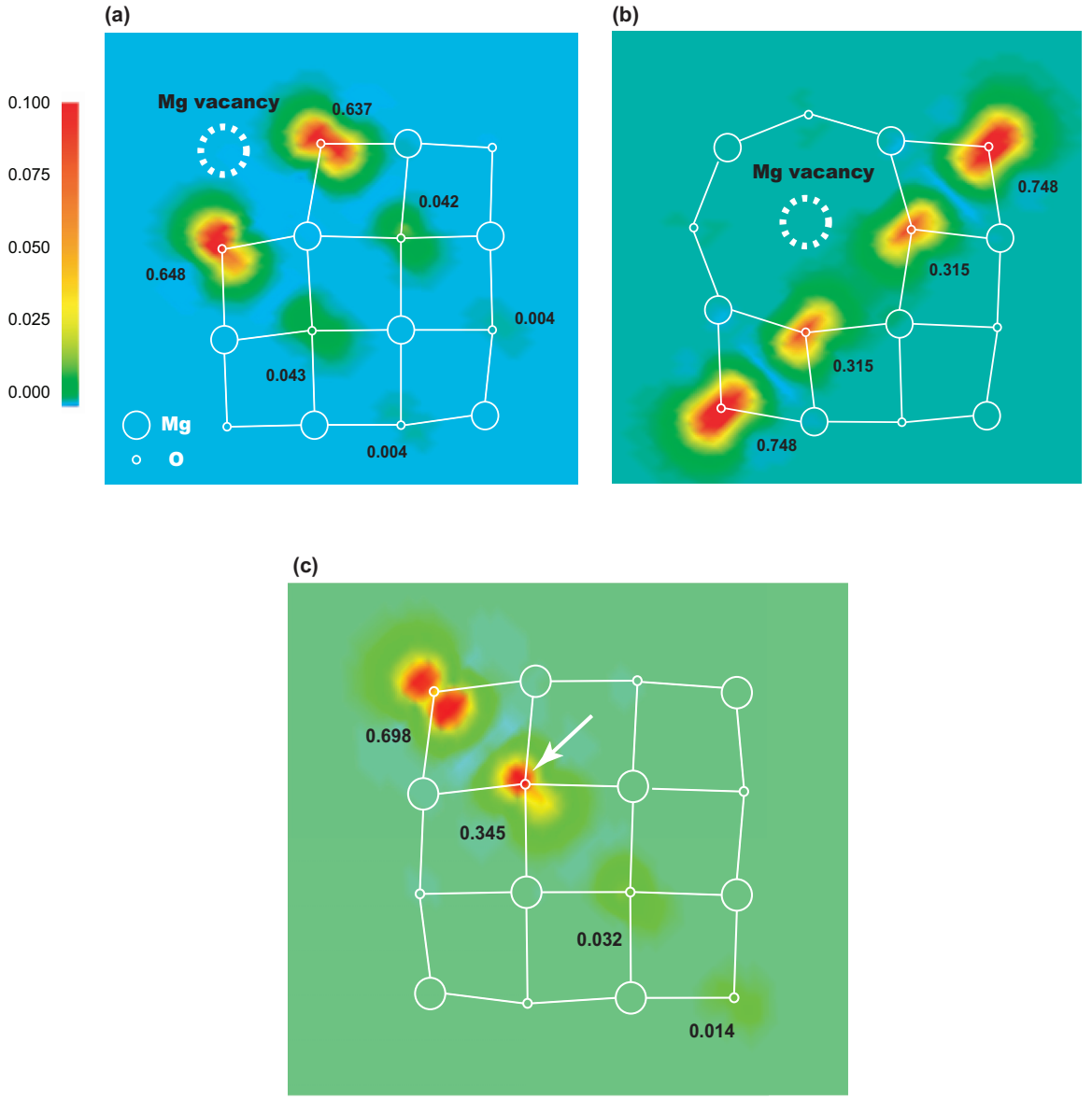

FIG. 5. (Color online) Spin-density map on one of the {100} planes for the $Mg_{31}O_{32}$ cluster in the spin-triplet state. The Mg vacancy is located (a) at the corner and (b) in the plane. In (c), the Mg vacancy resides at the subsurface or one layer below the oxygen atom indicated by the white arrow. Large and small circles represent Mg and O atoms, respectively. The values indicated are Mulliken atomic spin densities; the values below 0.001 are omitted.

in total energy by several electron volts than the spin-restricted singlet ($S = 0$) state. As far as the total energies are concerned, the spin-unrestricted singlet state is comparable to the spin-polarized $S \geqslant 1$ states. It should be noted, however, that the UDFT singlet states are always characterized by nonnegligible values of S^2 for all the Mg-deficient clusters employed in this work (see Tables I and II), hence showing spin contamination. This derives from the fact that UDFT determinant is not an eigenfunction of the total spin operator S^2 and inherently has the spin-impurity problem.[29] Thus, the total energy of the UDFT singlet state is affected by the spin-contamination effect and may not be used to evaluate the stability of the relevant spin states.

On the other hand, the spin-contamination problem can hardly be seen in the spin triplet ($S = 1$) and quintet ($S = 2$) states for the cluster with one and two Mg vacancies, respectively. It is hence most likely that the spin-polarized state with no spin contamination corresponds to the realistic spin state or the ground spin states for the respective Mg-deficient clusters. This allows us to expect that the total spin S of an MgO nanocrystal in the ground state scales with the number of Mg vacancies at the surface. It is therefore interesting to investigate whether the MgO clusters with three or more surface Mg vacancies yield a higher ($S \geqslant 3$) spin-ground state. To investigate the effect of the number of Mg vacancies on the ground state-spin configuration, we further employed a $(4 \times 4 \times 4)$-based cluster with four Mg vacancies at the four corners. We then performed full geometry optimization at the B3LYP/6-31G(d) level by assuming spin-restricted singlet, spin-unrestricted singlet, triplet, and nonet states.[30]

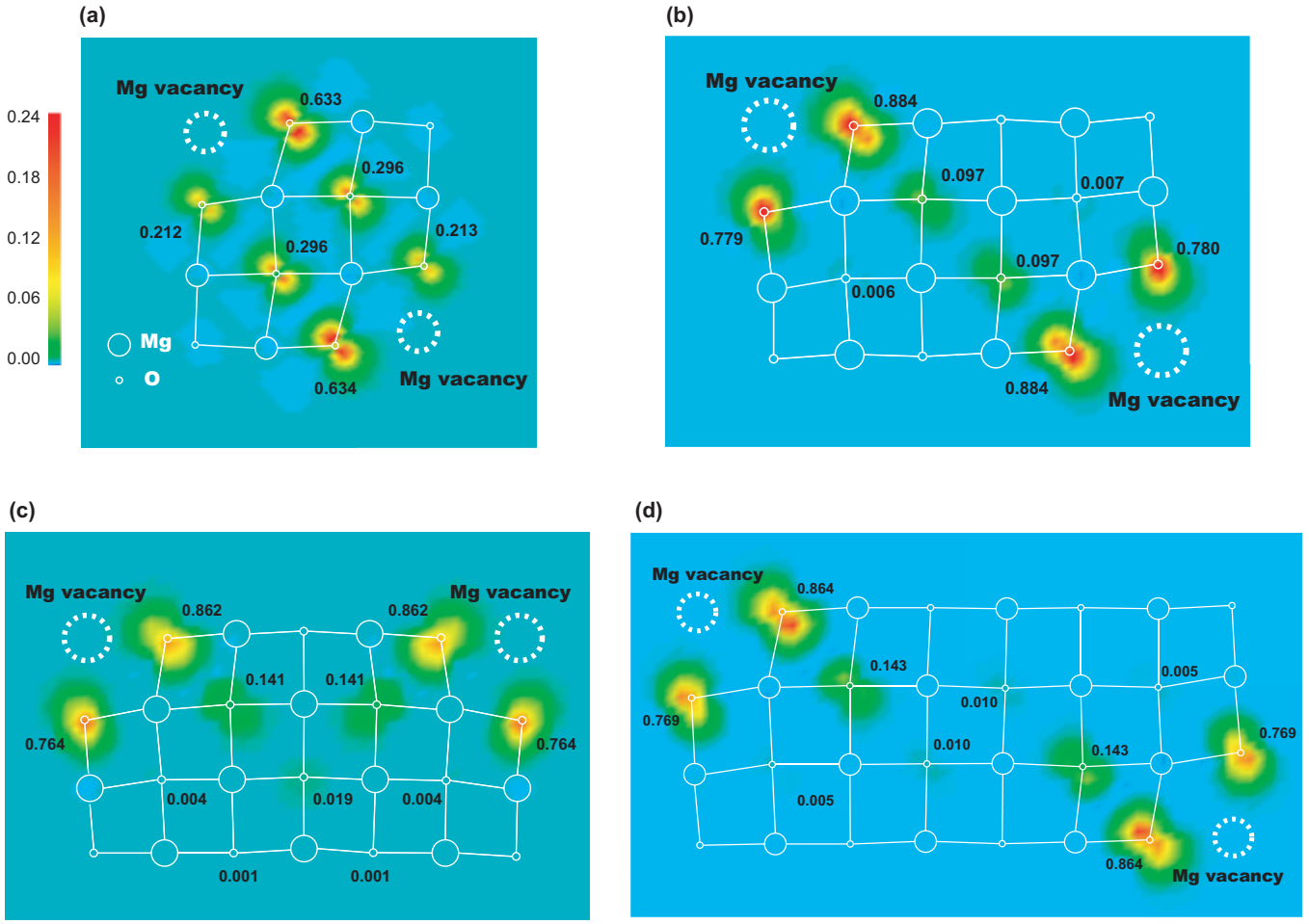

FIG. 6. (Color online) Spin-density map on the (100) plane containing two corner Mg vacancies calculated for the (a) (4 × 4 × 4)-, (b) (6 × 4 × 3)-, (c) (7 × 4 × 3)-, and (d) (8 × 4 × 3)-based clusters in the spin-quintet ($S = 2$) state. Large and small circles represent Mg and O atoms, respectively. The values indicated are Mulliken atomic spin densities; the values below 0.001 are omitted.

Table III compares the geometry-optimized total energies of the respective spin states. The $\langle S^2 \rangle$ values calculated for the spin nonoet ($S = 4$) state is 20.001 after annihilation of the first spin contaminant, showing an almost pure nonet state. Furthermore, the spin-nonet state was found to have the lowest total energy, although the total energies of the spin-unrestricted

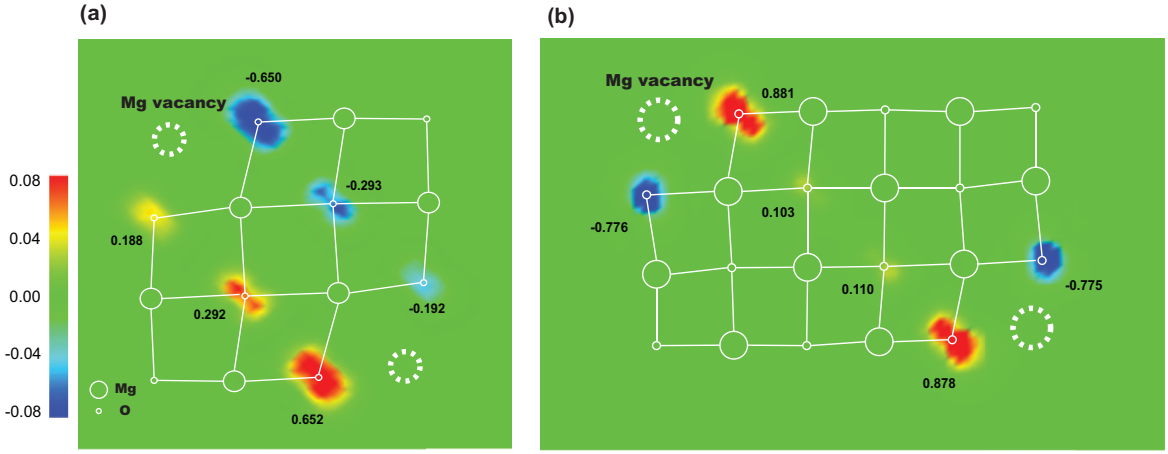

FIG. 7. (Color online) Spin-density map on the (100) plane containing two corner Mg vacancies calculated for the (a) (4 × 4 × 4)- and (b) (6 × 4 × 3)-based clusters in the spin-unrestricted singlet state. Large and small circles represent Mg and O atoms, respectively. The values indicated are Mulliken atomic spin densities; the values below ±0.1 are omitted.

TABLE III. Electronic properties of the (4 × 4 × 4)-based MgO cluster with four corner Mg vacancies optimized at the B3LYP/6-31G(d) level in the respective spin states.

Cluster	Spin State	ΔE[a](eV)	AE[b](eV)	$\langle S^2\rangle$[c]	$\Delta E_{\mathrm{H-L}}$[d](eV)
$Mg_{28}O_{32}$	singlet (R)[e]	–	242.511	0	0.50
(4 × 4 × 4)	singlet (U)[f]	−4.982	247.493	4.053 (12.307)	1.56 (α)/1.55(β)
	triplet	−4.933	247.444	5.053 (9.176)	1.73 (α)/1.49(β)
	nonet	−4.993	247.504	20.068 (20.001)	5.18 (α)/1.14(β)

[a] ΔE represents the total energy difference from the spin-restricted singlet state. Minus signs indicate that the total energy is lower than that of the spin-restricted singlet state.
[b] AE (Atomization Energy) $= mE(\mathrm{Mg}) + nE(\mathrm{O}) - E(\mathrm{Mg}_m\mathrm{O}_n)$, where $E(\mathrm{X})$ represents the total energy of the system X.
[c] The values in parentheses are those after annihilation of the first spin contaminant.
[d] $E_{\mathrm{H-L}}$ is the energy difference between the HOMO and the LUMO levels. α and β indicate the major and minor spin states, respectively.
[e] Spin-restricted singlet state.
[f] Broken-symmetry spin-unrestricted singlet state.

singlet and triplet states are only slightly higher than that of the spin-nonet state, similar to the case of the clusters with two Mg vacancies (see Table II). However, unrealistic $\langle S^2\rangle$ values, i.e., ∼12 and ∼9, were obtained for the UDFT singlet and triplet solutions, respectively, even after annihilation of the first spin contaminant. Thus, these spin sates are severely affected by mixing with a higher spin (nonet) state and cannot be regarded as a realistic spin state. The present results indicate that the effect of spin contamination becomes more serious and unavoidable with increasing the number of surface Mg vacancies.

Figure 8 shows the spin distribution of the nonet state of the cluster with four Mg vacancies at the corners. In this cluster, each {100} plane has basically the same spin distribution, showing a highly delocalized nature over surface O atoms along the ⟨110⟩ direction, in harmony with the results obtained for the cluster with two corner Mg vacancies [see Fig. 6(a)]. It follows that all the surfaces of the cluster with four corner Mg vacancies are characterized by delocalized spin density with the same spin orientation. A rather high stability of the spin-nonet state against the spin-singlet state most likely results from such a highly delocalized spin distribution around the surface of the cubic cluster.

From these calculations, we suggest that the observed magnetization of MgO nanocrystals scales with the number of Mg vacancies at the surface (or near surface). However, real MgO nanocrystals do not always have such ideal flat surfaces but are characterized by, depending on the synthetic conditions, different complex features such as terraces, steps, and kinks,[31] which most likely affect the resulting magnetization. This may induce the lack of reproducibility of d^0 ferromagnetic behavior, as indeed reported for a number of nanoscale oxides.

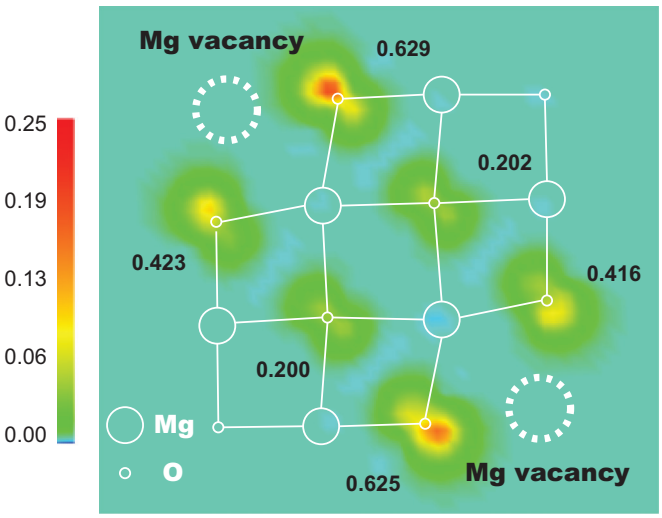

FIG. 8. (Color online) Spin-density map on one of the {100} planes for the $Mg_{28}O_{32}$ cluster in the spin-nonet ($S = 4$) state. The values indicated are Mulliken atomic spin densities; the values below 0.001 are omitted.

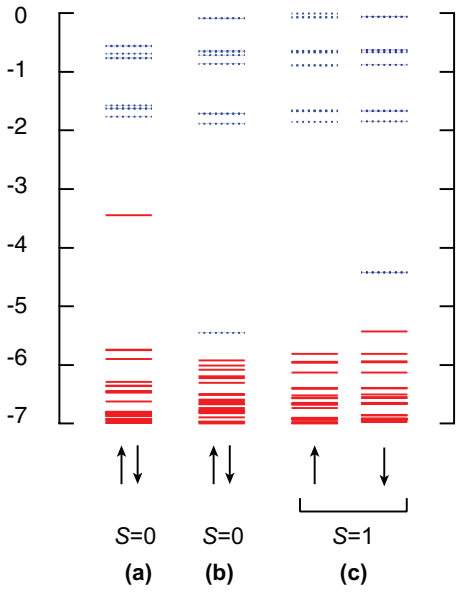

FIG. 9. (Color online) Molecular orbital energy-level diagrams of occupied molecular orbitals (solid lines) and unoccupied molecular orbitals (dotted lines) calculated for the (4 × 4 × 4)-based clusters with one O or one Mg vacancy at the corner. (a) O-deficient $Mg_{32}O_{31}$ cluster in the spin-singlet state, (b) Mg-deficient $Mg_{31}O_{32}$ cluster in the spin-singlet state, and (c) Mg-deficient $Mg_{31}O_{32}$ cluster in the spin-triplet state.

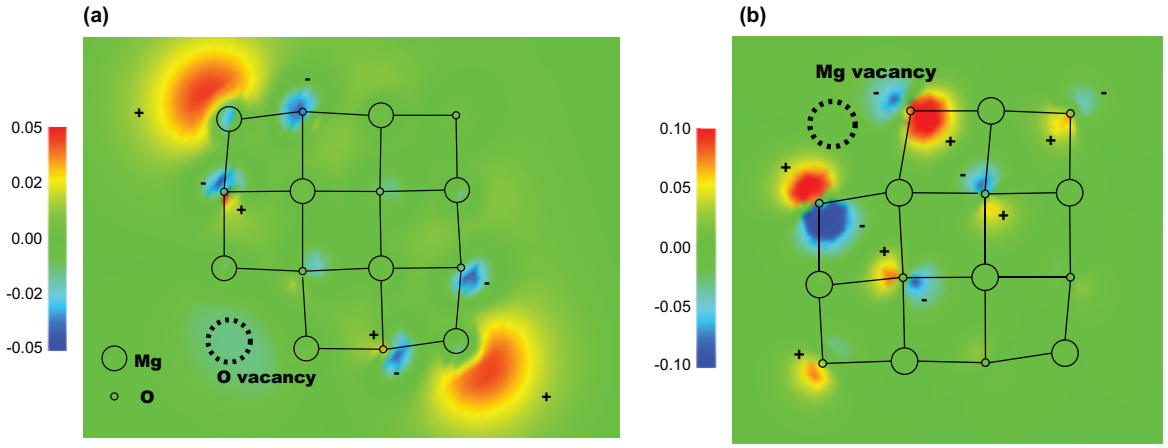

FIG. 10. (Color online) Cross section of the LUMO orbital of the $(4 \times 4 \times 4)$-based clusters with (a) one O vacancy and (b) one Mg vacancy at the corner calculated for the spin-restricted singlet state.

B. Origin of the spin-polarized ground state of the Mg-deficient clusters

Previously, a large number of cluster-based theoretical calculations have been performed to understand the surface-related properties of MgO.[32–36] To our knowledge, however, the spin-polarized ground state has not been predicted for any of the theoretical models including surface defects. This is probably because the electronic states of surface Mg vacancies, such as those treated in this paper, have not been seriously investigated. Previous studies[32–36] have been concerned mainly with surface sites with no vacancies, such as terraces, steps, and corners, and/or oxygen vacancies at the surface in view of their catalytic and luminescence activities.

The occurrence of the spin-polarized ground state for the present Mg-deficient clusters can be interpreted in terms of the molecular orbital diagrams of the respective clusters. We should note, however, that there has been substantial uncertainty as to the degree of physical significance of the Kohn Sham (KS) orbitals of DFT applied within the KS framework.[37] The above uncertainties notwithstanding, it has been demonstrated that KS orbitals obtained from hybrid functionals such as B3LYP generally have moderate accuracy and yield a systematic and predicted deviation from the corresponding experimental data, including the ionization potential and the electron affinity.[38] We hence consider that the comparison of the KS orbitals among the present series of the clusters is useful to understand the relative stability of their spin states.

Figure 9 shows the molecular orbital diagrams of the $(4 \times 4 \times 4)$-based clusters with one O or one Mg vacancy at the corner site in different spin states. As for the O-deficient cluster in the spin-restricted singlet state, the lowest unoccupied molecular orbital (LUMO) is higher in energy than the highest occupied molecular orbital (HOMO) by $\sim$1.7 eV [see Fig. 9(a)]. This contrasts with the case of the Mg-deficient cluster in the spin-restricted singlet state, where the LUMO is higher in energy than the HOMO only by $\sim$0.5 eV [see Fig. 9(b)]. Accordingly, spin-unrestricted sates are naturally expected in the Mg-deficient cluster because of the small HOMO-LUMO gap, which costs less energy to flip a spin, leading to the spin polarized ($S = 1$) lower-energy state [see Fig. 9(c)]. Such a small ($\sim$0.5 eV) HOMO-LUMO gap is observed for all the Mg-deficient clusters in the spin-restricted singlet state (see Tables I and II).

The following question then naturally arises: Why does the Mg-deficient cluster have such a small HOMO-LUMO gap in the spin-restricted singlet state? It is clear from Fig. 9 that the difference in the HOMO-LUMO gap between the O- and Mg-deficient clusters in their spin-restricted singlet state results mainly from the degree of stabilization of the LUMO level. We hence compare the corresponding unoccupied orbitals for the Mg- and O-deficient clusters. As shown in Fig. 10, the LUMO of the O-deficient cluster in the spin-restricted singlet state is localized mainly on the corner Mg atoms. On the other hand, the LUMO of the Mg-deficient cluster in the spin-restricted singlet state spreads over several O atoms in the $\langle 110 \rangle$ directions at the surface, similar to the case of the spin distribution in the triplet state (see Fig. 5). It is hence most likely that the stabilization of the LUMO level obtained for the Mg-deficient cluster in the spin-restricted singlet state originates from a highly delocalized nature of the LUMO. Accordingly, as noted in Sec. III A, these surface O atoms contributing to the LUMO level can provide a shallow acceptor level, eventually allowing a spin flip to result in a spin-polarized ground state.

V. CONCLUSIONS

We have shown from a series of DFT calculations on MgO nanoclusters that the Mg vacancies at the surface or near surface can induce a delocalized spin distribution over several neighboring surface O atoms along the $\langle 110 \rangle$ directions. This directional spin delocalization enables a pair of distant ($\sim$1 nm or longer) Mg vacancies to interact ferromagnetically. The total energy of the resulting magnetic state is lower than that of a nonmagnetic by several electron volts, leading to the robust spin-polarized ground state. Among other Mg vacancies, those at corners have been shown to be most energetically favorable

ones. We have further demonstrated that the total spin S of the clusters in their ground state is equal to the number of Mg vacancies at the surface. These results allow us to suggest that surface Mg vacancies along with the low-coordinated surface O atoms are prerequisite for long-range ferromagnetic interaction, hence providing a delocalized mediating state or a percolation network for surface defect-related ferromagnetism in nanoscale magnesium oxides.

We thank the Supercomputer System, Institute for Chemical Research, Kyoto University, for providing the computer time to use the SGI UV 100 supercomputer.

*Author to whom correspondence should be addressed: uchino@kobe-u.ac.jp

[1] J. M. D. Coey, Solid State Sci. **7**, 660 (2005).
[2] M. Venkatesan, C. B. Fitzgerald, and J. M. D. Coey, Nature (London) **430**, 630 (2004).
[3] S. D. Yoon, Y. Chen, A. Yang, T. L. Goodrich, X. Zuo, D. A. Arena, K. Ziemer, C. Vittoria, and V. G. Harris, J. Phys.: Condens. Matter **18**, L355 (2006).
[4] N. H. Hong, J. Sakai, N. Poirot, and V. Brizé, Phys. Rev. B **73**, 132404 (2006).
[5] A. Sundaresan, R. Bhargavi, N. Rangarajan, U. Siddesh, and C. N. R. Rao, Phys. Rev. B **74**, 161306(R) (2006).
[6] J. Hu, Z. Zhang, M. Zhao, H. Qin, and M. Jiang, Appl. Phys. Lett. **93**, 192503 (2008).
[7] C. Martínez-Boubeta, J. I. Beltrán, L. Balcells, Z. Konstantinović, S. Valencia, D. Schmitz, J. Arbiol, S. Estrade, J. Cornil, and B. Martinez, Phys. Rev. B **82**, 024405 (2010).
[8] B. M. Maoz, E. Tirosh, M. Bar Sadan, and G. Markovich, Phys. Rev. B **83**, 161201(R) (2011).
[9] M. Stoneham, J. Phys.: Condes. Matter **22**, 074211 (2010).
[10] S. B. Ogale, Adv. Mater. **22**, 3125 (2010).
[11] J. M. D. Coey and S. A. Chambers, MRS Bull. **33**, 1053 (2008).
[12] G. Xing, D. Wang, J. Yi, L. Yang, M. Gao, M. He, J. Yang, J. Ding, T. C. Sum, and T. Wu, Appl. Phys. Lett. **96**, 112511 (2010).
[13] A. Kumar, J. Kumar, and S. Priya, Appl. Phys. Lett. **100**, 192494 (2012).
[14] J. A. Chan, S. Lany, and A. Zunger, Phys. Rev. Lett. **103**, 016404 (2009).
[15] A. Droghetti, C. D. Pemmaraju, and S. Sanvito, Phys. Rev. B **81**, 092403 (2010).
[16] A. Zunger, S. Lany, and H. Raebiger, Physics **3**, 53 (2010).
[17] T. Uchino and T. Yoko, Phys. Rev. B **85**, 012407 (2012).
[18] F. Wang, Z. Pang, L. Lin, S. Fang, Y. Dai, and S. Han, Phys. Rev. B **80**, 144424 (2009).
[19] S. Veliah, R. Pandey, Y. S. Li, J. M. Newsam, and B. Vessal, Chem. Phys. Lett. **235**, 53 (1995).
[20] E. Antoshchenkova, M. Hayoun, G. Geneste, and F. Finocchi, PhysChemChemPhys **12**, 7251 (2010).
[21] N. Kumar, D. Sanyal, and A. Sundaresan, Chem. Phys. Lett. **477**, 360 (2009).
[22] S. T. Bromley, I. de P. R. Moreira, K. M. Neyman, and F. Illas, Chem. Soc. Rev. **38**, 2657 (2009).
[23] A. D. Becke, J. Chem. Phys. **98**, 5648 (1993).
[24] C. Lee, W. Yang, and R. G. Parr, Phys. Rev. B **37**, 785 (1988).
[25] M. J. Frisch, G. W. Trucks, H. B. Schlegel, G. E. Scuseria, M. A. Robb, J. R. Cheeseman, G. Scalmani, V. Barone, B. Mennucci, G. A. Petersson, H. Nakatsuji, M. Caricato, X. Li, H. P. Hratchian, A. F. Izmaylov, J. Bloino, G. Zheng, J. L. Sonnenberg, M. Hada, M. Ehara, K. Toyota, R. Fukuda, J. Hasegawa, M. Ishida, T. Nakajima, Y. Honda, O. Kitao, H. Nakai, T. Vreven, J. A. Montgomery, Jr., J. E. Peralta, F. Ogliaro, M. Bearpark, J. J. Heyd, E. Brothers, K. N. Kudin, V. N. Staroverov, R. Kobayashi, J. Normand, K. Raghavachari, A. Rendell, J. C. Burant, S. S. Iyengar, J. Tomasi, M. Cossi, N. Rega, J. M. Millam, M. Klene, J. E. Knox, J. B. Cross, V. Bakken, C. Adamo, J. Jaramillo, R. Gomperts, R. E. Stratmann, O. Yazyev, A. J. Austin, R. Cammi, C. Pomelli, J. W. Ochterski, R. L. Martin, K. Morokuma, V. G. Zakrzewski, G. A. Voth, P. Salvador, J. J. Dannenberg, S. Dapprich, A. D. Daniels, O. Farkas, J. B. Foresman, J. V. Ortiz, J. Cioslowski, and D. J. Fox, GAUSSIAN 09, Revision A.02 (Gaussian, Inc., Wallingford, 2009).
[26] M. Pesci, F. Gallino, C. Di Valentin, and G. Pacchioni, J. Phys. Chem. C **114**, 1350 (2010).
[27] G. Pacchioni, F. Frigoli, D. Ricci, and J. A. Weil, Phys. Rev. B **63**, 054102 (2000).
[28] F. Gao, J. Hu, C. Yang, Y. Zheng, H. Qin, L. Sun, X. Kong, and M. Jiang, Solid State Commun. **149**, 855 (2009).
[29] A. J. Cohen, D. J. Tozer, and N. C. Handy, J. Chem. Phys. **126**, 214104 (2007).
[30] Geometry optimization was also performed by assuming spin quintet ($S = 2$) and septet ($S = 3$) states, but the SCF did not converge even after 300 iterations. Thus, we did not obtain the optimized structure for these spin states.
[31] E. Knözinger, K.-H. Jacob, S. Singh, and P. Hofmann, Surf. Sci. **290**, 388 (1993).
[32] A. M. Ferrari and G. Pacchioni, J. Phys. Chem. **99**, 17010 (1995).
[33] A. L. Shluger, P. V. Sushko, and L. N. Kantorovich, Phys. Rev. B **59**, 2417 (1999).
[34] P. V. Sushko, J. L. Gavartin, and A. L. Shluger, J. Phys. Chem. B **106**, 2269 (2002).
[35] D. Ricci, C. Di Valentin, G. Pacchioni, P. V. Sushko, A. L. Shluger, and E. Giamello, J. Am. Chem. Soc. **125**, 738 (2003).
[36] A. Sternig, D. Koller, N. Siedl, O. Diwald, and K. McKenna, J. Phys. Chem. C **116**, 10103 (2012).
[37] See, for example, C. J. Cramer, *Essentials of Computational Chemistry*, 2nd ed. (Wiley, Hoboken, 2004).
[38] G. Zhang and C. B. Musgrave, J. Phys. Chem. A **111**, 1554 (2007).